

THE KINEMATICS OF MOLECULAR OUTFLOWS

STEVEN W. STAHLER

Astronomy Department, University of California, Berkeley, CA 94720; and NASA-Ames Research Center

Received 1993 June 4; accepted 1993 August 23

ABSTRACT

If molecular outflows represent turbulent material entrained by a central jet, then the surfaces of constant velocity should spread outward from the jet axis. Using the results of CO observations, I propose an empirical velocity distribution of this character. Outflows with this distribution display the well-documented “acceleration” phenomenon, i.e., the increase in terminal velocity away from the driving star.

Subject headings: ISM: jets and outflows — ISM: kinematics and dynamics — stars: formation

1. INTRODUCTION

One of the most conspicuous ways young stars affect their environments is through the production of bipolar molecular outflows (recent reviews include Bally & Lane 1991; Padman, Lasenby, & Green 1991; Cabrit 1993; Bachiller & Gómez-González 1992). It is generally accepted that the outflow lobes consist of ambient cloud material set into motion by a stellar wind. However, the exact nature of the wind-cloud interaction remains obscure, reflecting a basic uncertainty regarding the spatial disposition of the moving molecular gas. In their pioneering study of L1551/IRS 5, Snell, Loren, & Plambeck (1980) interpreted the observed CO emission as arising from relatively thin, dense shells enclosing nearly vacuous inner cavities. These cavities were presumed to be cleared by the wind as it sweeps up the surrounding cloud material. This hollow shell model has largely dominated subsequent research, although serious discrepancies with observations have been noted (Cabrit & Bertout 1986; Levreault 1988b; Masson & Chernin 1992).

From a more general standpoint, a weakness of the traditional model is that it has failed to relate outflows in a convincing way to another bipolar phenomenon exhibited by young stars, the Herbig-Haro jets (Reipurth 1991). This failure has been underscored by the discovery of a new class of tightly collimated, high-velocity flows, for which a windblown cavity model is clearly inappropriate (Bachiller et al. 1990; André et al. 1990; Richer, Hills, & Padman 1992). In response to these difficulties, an alternative, radically different picture of outflows has emerged. Here, the lobes are seen as *filled* with turbulent molecular gas. This gas has been entrained by a central, high-velocity jet, which itself consists of stellar wind material propagating to large distances in a relatively narrow structure (see Stahler 1993 for an exposition of this view). To date, there has been little attempt to draw quantitative conclusions or predictions, but the first theoretical descriptions of the momentum transfer from the jet to the surrounding cloud have now appeared (Masson & Chernin 1993; Raga et al. 1993). My purpose here is to show how the new perspective sheds light on the velocity structure of outflows, and on their apparent *acceleration* from the central stars.

For any outflow observed in a particular CO transition, the acceleration is most evident in a position-velocity diagram constructed along the lobes' central axes. If $I_{\text{CO}}(v, x)$ denotes the line intensity at radial velocity v , and position x along the axis from the star, then such diagrams display this function by plotting contours of constant I_{CO} . Several examples are shown

in Figure 1, where the position coordinates are given as angular displacements. Included in the figure are L1551/IRS 5 (see Fig. 1a) and NGC 2264G (see Fig. 1b), both exhibiting modest collimation, and VLA 1623, one of the narrower, high-velocity systems (see Fig. 1c).

In each diagram, there is a thick ridge of strong emission running along the x -axis. This ridge (which was deleted for clarity in Fig. 1c) represents ambient cloud material with essentially zero radial velocity. Outside this region, the intensity contours first fan out with increasing distance from the driving star, then eventually retreat toward the axis further downstream. That is, the maximum radial velocity, as well as the mean value, both *increase* initially. The effect is most evident in those outflow systems with clearly separated red- and blue-shifted lobes, i.e., the ones lying nearly in the plane of the sky (Cabrit 1993).

What is causing the velocity increase? If the lobes are indeed filled with turbulent gas, then explanations based on ballistic motion or acceleration of gas parcels through an empty cavity must be rejected. Under the entrainment hypothesis, material in the cloud is being dragged forward by the underlying, central jet. In laboratory flows, this process sets up a characteristic spreading of velocities in the turbulent region outside the laminar core of the jet (Abramovich 1963). In § 2 below, I first argue that the measured column densities in outflows indicate a velocity distribution of just this type. Then, in § 3, I check the validity of the empirical distribution by constructing a generic position-velocity diagram close to the driving star. This diagram displays the desired fanlike structure. Finally, § 4 discusses the broader significance of this result.

2. VELOCITY DISTRIBUTION

For clouds observed with optically thin lines, the intensity integrated over any velocity interval is directly proportional to the column density in that interval and spatial location. The $^{12}\text{CO } J = 1 \rightarrow 0$ transition used most frequently in outflow studies has a modest optical depth at all but the lowest velocities, so that the column density can still be reconstructed (e.g., Moriarty-Schieven & Snell 1988). Thus, in a fully mapped outflow, the total mass at each radial velocity can be obtained by summation. The results of this exercise are instructive, and are shown for four cases in Figure 2. It should be recalled here that, in the new picture, the measured radial velocity represents, to within a projection factor, the mean *forward* motion of each element in the turbulent flow. The mean *lateral* motion

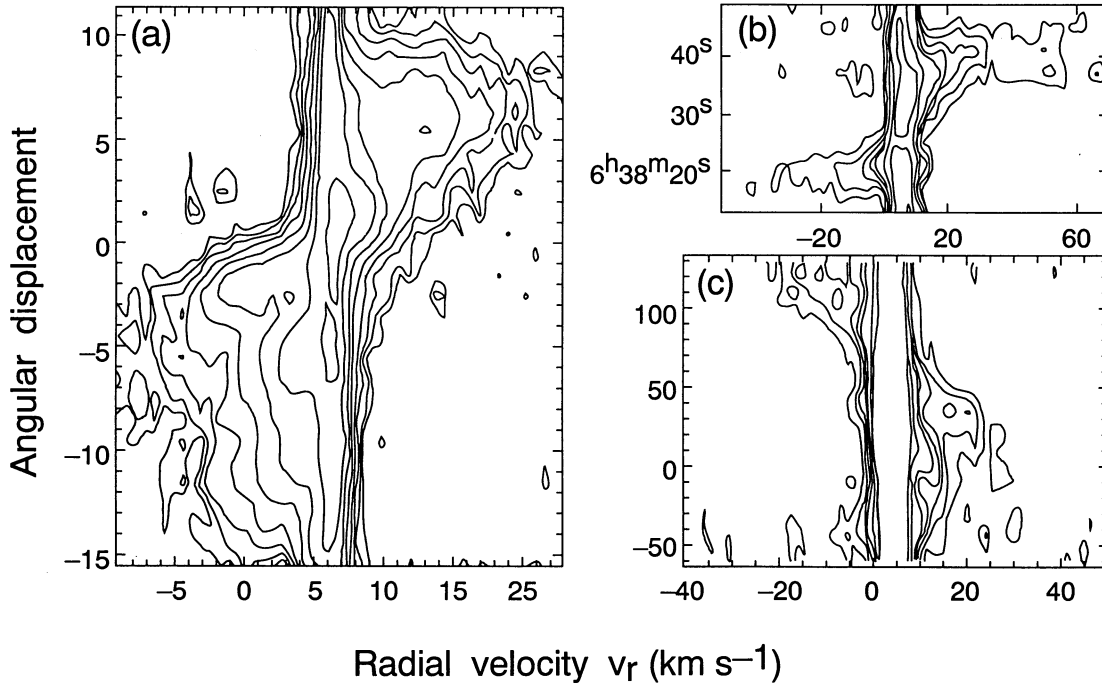


FIG. 1.—Position-velocity diagrams along the central outflow axes for (a) L1551/IRS 5 (Levreault 1988a), (b) NGC 2264G (Margulis et al. 1990), and (c) VLA 1623 (André et al. 1990). The units for angular displacement are arcminutes in (a), and arcseconds for (b) and (c). The L1551/IRS 5 diagram was constructed using the ^{12}CO $J = 2 \rightarrow 1$ line, while the others used the $J = 1 \rightarrow 0$ transition.

away from the jet axis is presumed to be negligible (Meyers-Rice & Lada 1991).¹

Figure 2 indicates that the bulk of the mass in any lobe is moving at relatively low speeds. This fact was known earlier from detailed studies of individual outflow systems (e.g., Moriarty-Schieven, Snell, & Hughes 1989). More significantly for our purposes, the figure also shows that the falloff of mass with velocity is remarkably similar in all examples, including VLA 1623, for which the total outflow mass is several orders of magnitude less than for the others. Let $M(v)$ be the amount of mass in any lobe with forward velocity from v_{\min} to v . Here v_{\min} is the ambient value evident in the central ridges of Figure 1, to be identified with the velocity dispersion in areas well removed from the outflow. Then we have the empirical result

$$\frac{dM(v)}{dv} = k \left(\frac{v}{v_j} \right)^{-\gamma}, \quad (1)$$

where γ is ~ 1.9 , and where k is a different constant for each outflow. The velocity v_j in this equation is a fiducial jet speed, introduced for later convenience. Since we have no reason to expect equation (1) to hold for speeds close to v_j , its range of validity is $v_{\min} < v \ll v_j$.

Now the outflows shown in Figure 2 vary greatly in lobe length, degree of collimation, and total mechanical power. It is implausible, therefore, that a *global* relation such as equation (1) could hold unless there were an underlying *local* relation, as well. Specifically, we expect the falloff of mass with velocity to be valid in every slab of gas perpendicular to the jet axis (see

¹ More precisely, it is assumed that the line-of-sight projection of the forward velocity dominates the projected lateral velocity, even for outflows nearly in the plane of the sky. That *some* lateral motion exists is apparent, for example, in the admixture of blueshifted emission seen in the red lobe of VLA 1623 (Fig. 1c).

Fig. 3). In mathematical terms, we posit

$$m(v, x) = \kappa(x) \left(\frac{v}{v_j} \right)^{-\gamma}. \quad (2)$$

Here, $m(v, x)\Delta v\Delta x$ is the amount of mass in the slab located between x and $x + \Delta x$, and with forward velocity between $v + \Delta v$. The quantities $m(v, x)$ and $M(v)$ are related by

$$\int_{v_{\min}}^v dv \int_0^L dx m(v, x) = M(v)$$

in an outflow of length L . An outflow in which equation (2) holds everywhere also obeys the global relation (1) provided that

$$k = \int_0^L \kappa(x) dx.$$

Equation (2) can be used to derive the velocity distribution in the outflow. In Figure 3, the volume of the annulus of radius r , width Δr , and thickness Δx is $2\pi r\Delta r\Delta x$. Thus, $m(v, x)$ can also be written as

$$m(v, x) = -2\pi r \left(\frac{\partial r}{\partial v} \right)_x \rho(x), \quad (3)$$

where the minus sign accounts for the fact that we expect the partial derivative to be negative, and where the mass density ρ has been allowed to vary with distance from the star. Combining equations (2) and (3), we find

$$\left(\frac{v}{v_j} \right)^{-\gamma} \left(\frac{\partial v}{\partial r} \right)_x = - \frac{2\pi r \rho(x)}{\kappa(x)}. \quad (4)$$

Equation (4) admits a particularly simple type of solution for the velocity, in which v depends on the single independent variable $\eta \equiv r/g(x)$. The function $g(x)$ describes the shape of the

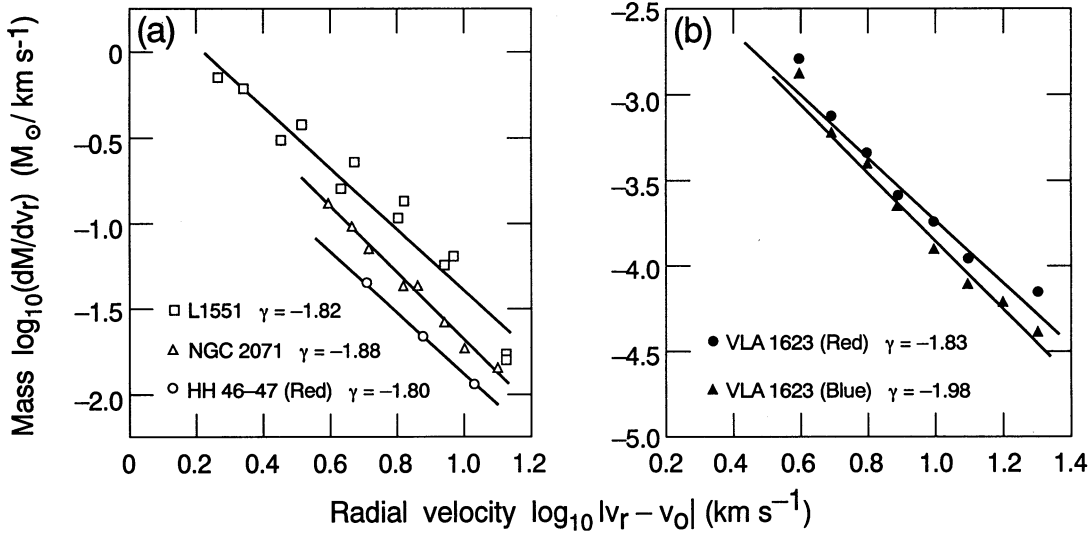


FIG. 2.—Observed mass distributions for four outflows. Plotted is the integrated mass per unit radial velocity. The horizontal axis is the absolute value of the radial velocity v , minus v_0 , the velocity at line center. Panel *a* is taken from Masson & Chernin (1992), who cite the original references. Panel *b* is from André (1993, private communication). Note that the velocity distributions for L1551/IRS 5 and NGC 2071 are integrated over both outflow lobes, while the other distributions refer to individual lobes, as indicated.

outflow lobe, i.e., it is proportional to the distance, at each x , from the central axis to the point where the velocity falls to v_{\min} . We now write the velocity in the form

$$v = v_j f(\eta)$$

and substitute into equation (4). After some manipulation, we obtain

$$\frac{f^{-\gamma} f'(\eta)}{\eta} = -\frac{2\pi}{v_j} \frac{\rho(x) g^2(x)}{\kappa(x)}. \quad (5)$$

Since x and η are independent variables, equation (5) can only be satisfied if both sides are equal to a constant, which we

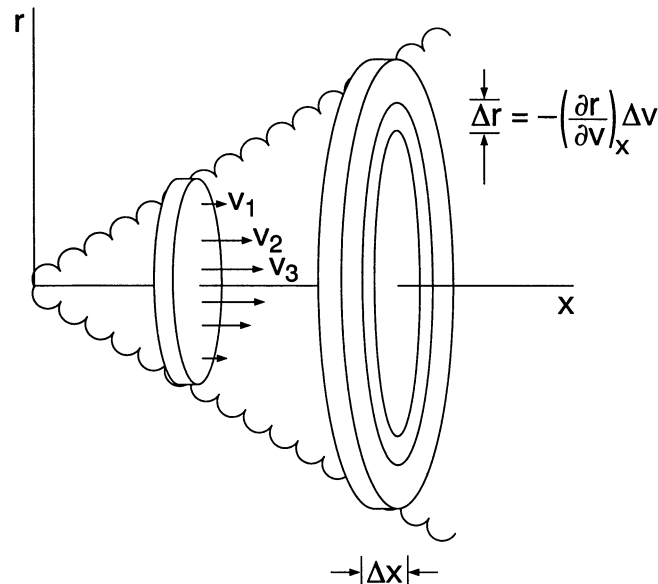


FIG. 3.—Velocity distribution within outflows (schematic). Within each slab, of thickness Δx , the forward velocity v falls off from the central axis. Thus, $v_3 > v_2 > v_1$. Each annulus of width Δr is associated with a certain velocity in the interval Δv , where $\Delta r = -(\partial r/\partial v)_x \Delta v$.

denote as $-\lambda$, for λ assumed positive. We thus have the two additional equations

$$f'(\eta) = -\lambda \eta f^\gamma \quad (6a)$$

$$\kappa(x) = \frac{2\pi}{\lambda v_j} \rho(x) g^2(x). \quad (6b)$$

We integrate equation (6a), subject to the condition that f be unity at $\eta = 0$. The result is

$$f = \left[1 + \frac{\lambda(\gamma - 1)}{2} \eta^2 \right]^{-1/(\gamma - 1)}. \quad (7)$$

This latter relation, being based on equation (2), is really only valid in the regime where the second term in the braces is much larger than unity. We thus arrive at the velocity distribution

$$v = v_* \eta^{-2/(\gamma - 1)}, \quad v_{\min} < v \ll v_j, \quad (8)$$

where v_* is a fiducial velocity for the particular system.

3. POSITION-VELOCITY DIAGRAM

Let us denote by $I(v, x)$ the column density in the flow along any line of sight measured per unit velocity. We have previously noted that this quantity is proportional to the received intensity $I_{\text{CO}}(v_r, x)$ in the optically thin approximation. Figure 4 illustrates that, for an outflow lying nearly in the plane of the sky, $I(v, x)$ is given by

$$I(v, x) = -\rho \left(\frac{\partial r}{\partial v} \right)_x.$$

Using equation (4), we find that

$$I(v, x) = \frac{\kappa(x)}{2\pi \eta g(x)} \left(\frac{v}{v_j} \right)^{-\gamma},$$

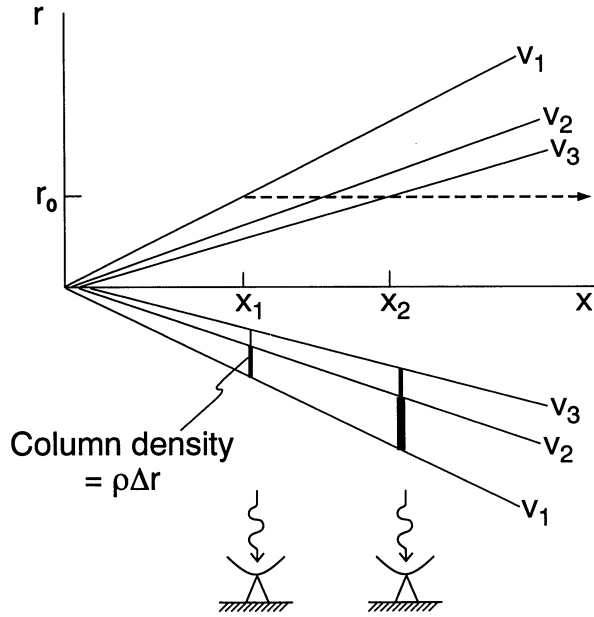


FIG. 4.—Velocity contours in outflows (schematic). The solid cones, centered on the jet axis, represent surfaces of constant forward velocity. As in Fig. 3, $v_3 > v_2 > v_1$, and we suppose additionally that $v_3 - v_2 = v_2 - v_1$. The dashed line is the path of a fluid element that starts at $x = x_1$, $r = r_0$. The vertical line segments represent the columns of material, along the two lines of sight shown, that are present between the indicated velocities. The thickness of each vertical line varies directly with the value of the column density.

which becomes, after using equations (6b) and (8),

$$I(v, x) = \frac{1}{\lambda v_j} \rho(x)g(x) \left(\frac{v}{v_j}\right)^{-\gamma} \eta^{-1} \quad (9a)$$

$$= \frac{\rho(x)g(x)}{\mu} \left(\frac{v}{v_*}\right)^{-(1+\gamma)/2}, \quad (9b)$$

where μ is another constant.

The functions $\rho(x)$ and $g(x)$ must be obtained observationally or from a solution to the full dynamical problem. If we

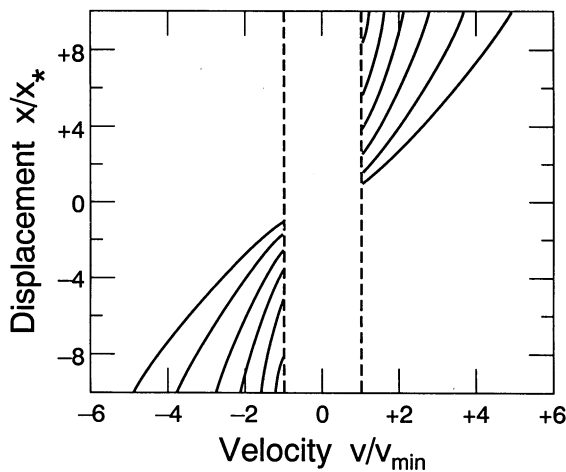


FIG. 5.—Synthetic position-velocity diagram along the central outflow axis. The diagram is for an outflow nearly in the plane of the sky and uses the forward, rather than radial, velocity. The figure was constructed using eq. (11), with γ set equal to 1.9. Contour levels (solid curves) are spaced by a factor of 1.5 in intensity. No contours are shown within the two vertical dashed lines, which represent the velocity dispersion of the cloud matter far from the outflow.

focus our interest on the region close to the start of the outflow, both functions can be expanded in powers of x :

$$g(x) = g'(0)x + \mathcal{O}(x^2),$$

$$\rho(x) = \rho(0) + \rho'(0)x + \mathcal{O}(x^2).$$

Substituting these expansions into equation (9b), and retaining only the terms of lowest order, we obtain

$$I(v, x) = \frac{\rho(0)g'(0)x}{\mu} \left(\frac{v}{v_j}\right)^{-(1+\gamma)/2}. \quad (10)$$

We define a standard intensity I_* and position x_* , such that $I(v_{\min}, x_*) = I_*$. Then equation (10) can be inverted to yield a form more appropriate for a position-velocity diagram:

$$v = v_{\min} \left(\frac{x}{x_*}\right)^{2/(1+\gamma)} \left(\frac{I}{I_*}\right)^{-2/(1+\gamma)}. \quad (11)$$

This last relation is plotted as Figure 5, for a number of values of the ratio I/I_* . Despite the simplicity of the derivation, in which such factors as beam dilution, finite optical depth, and turbulent broadening have been neglected, it can be seen that the basic pattern of spreading contours seen in Figure 1 is reproduced.

4. DISCUSSION

Near the start of an outflow lobe, equation (8) implies that v is proportional to $(r/x)^{-2/(\gamma-1)}$. That is, the surfaces of constant forward velocity are cones centered on the jet axis. Such conical surfaces are a characteristic feature of the turbulent region surrounding jets in the laboratory (Abramovich 1963, chap. 1; Landau & Lifshitz 1975, chap. 3). Most of the experiments concern subsonic jets entering an incompressible medium, but a conical pattern of turbulence also appears in the supersonic case (see Cantó & Raga 1991, and references therein). The laboratory analogy thus serves to emphasize the role of the central jet in establishing, through entrainment, the velocity distribution within outflows.

We now return to the question posed at the beginning: What causes the acceleration seen along the central axis? The mathematical answer is embodied in equation (11), but it is also instructive to view the solution in more physical terms. Figure 4 shows that an observer looking at distance x_1 from the star sees a relatively small column density of material between v_2 and v_3 , which, we suppose, is just below the detector's sensitivity limit (The column densities are indicated by the thickness of the short vertical lines). If we assume that $v_3 - v_2 = v_2 - v_1$, then the column between v_1 and v_2 is greater, and is barely detectable. At position x_2 , the thickening of the sheath of matter between v_2 and v_3 has now created a sufficient column density for detection, while the intensity between v_1 and v_2 is even greater. The net result is that material with progressively higher velocities comes into view at greater displacements from the star.

In this picture, the full velocity range, from v_{\min} to v_j , is present at all x -positions. Nevertheless, it should be emphasized that the spreading velocity pattern does represent a true acceleration in the direction of the jet. Consider, as in Figure 4, a fluid element located at x_1 , a distance r_0 from the axis. The forward motion of the element, initially at velocity v_1 , carries it to regions where its speed increases, first to v_2 , and then, by position x_2 , to v_3 . Acceleration is caused by the turbulent drag exerted by underlying, faster moving material. Ultimately, this

material must tap the momentum source provided by the central jet.

Acceleration of turbulent matter is but one facet of the entrainment process. The other main aspect is the replenishment, from the outside, of the material dragged forward by the jet. This replenishment occurs through subsonic motion in the laminar region surrounding the turbulence (Landau & Lifshitz 1975, chap. 3). The draining of cloud material at large distances is a promising mechanism for rendering embedded young stars optically visible and will be explored quantitatively in a future study.

It is a pleasure to thank R. Bachiller, C. Masson, and J. Richer for fruitful discussions, and A. Königl and F. Wilkin for comments on the manuscript prior to submission. I am especially grateful to P. André, both for his ongoing interest and for supplying the unpublished data on VLA 1623 that appears in Figure 2. This project was supported principally by NSF Grant AST-9296096. Additional funding was provided by the Center for Star Formation Studies, a consortium of U. C. Berkeley, U. C. Santa Cruz, and Nasa-Ames Research Center, supported through a special NASA astrophysics theory grant.

REFERENCES

- Abramovich, G. N. 1963, *The Theory of Turbulent Jets* (Cambridge: MIT Press)
- André, P., Martin-Pintado, J., Despois, D., & Montmerle, T. 1990, *A&A*, 236, 180
- Bachiller, R., Cernicharo, J., Martin-Pintado, J., Tafalla, M., & Lazareff, B. 1990, *A&A*, 231, 174
- Bachiller, R., & Gómez-González, J. 1992, *Astron. Astrophys. Rev.*, 3, 257
- Bally, J., & Lane, A. P. 1991, in *Physics of Star Formation and Early Stellar Evolution*, ed. C. J. Lada & N. Kylafis (Dordrecht: Kluwer), 471
- Cabrit, S. 1993, in *Stellar Jets and Bipolar Outflows*, ed. L. Errico and A. A. Vittone (Dordrecht: Kluwer), 1
- Cabrit, S., & Bertout, C. 1986, *ApJ*, 307, 313
- Cantó, J., & Raga, A. C. 1991, *ApJ*, 372, 646
- Landau, L. D., & Lifshitz, E. M. 1975, *Fluid Mechanics* (Oxford: Pergamon)
- Levreault, R. M. 1988a, *ApJS*, 67, 283
- . 1988b, *ApJ*, 330, 897
- Margulis, M., Lada, C. J., Hasegawa, T., Hayashi, S. S., Hayashi, M., Kaifu, N., Gatley, I., Greene, T. P., & Young, E. T. 1990, *ApJ*, 352, 615
- Masson, C. R., & Chernin, L. M. 1992, *ApJ*, 387, L47
- . 1993, *ApJ*, 414, 230
- Meyers-Rice, B., & Lada, C. J. 1991, *ApJ*, 368, 445
- Moriarty-Schieven, G. H., & Snell, R. L. 1988, *ApJ*, 332, 364
- Moriarty-Schieven, G. H., Snell, R. L., & Hughes, 1989, *ApJ*, 347, 358
- Padman, R., Lasenby, A. N., & Green, D. A. 1991, in *Beams and Jets in Astrophysics*, ed. A. Hughes (New York: Cambridge Univ. Press), 484
- Raga, A. C., Cantó, J., Calvet, N., Rodríguez, L. F., & Torrelles, J. M. 1993, preprint
- Reipurth, B. 1991, in *Physics of Star Formation and Early Stellar Evolution*, ed. C. J. Lada and N. Kylafis (Dordrecht: Kluwer), 497
- Richer, J. S., Hills, R. E., & Padman, R. 1992, *MNRAS*, 254, 525
- Snell, R. L., Loren, R. B., & Plambeck, R. L. 1980, *ApJ*, 239, L17
- Stahler, S. W. 1993, in *Astrophysical Jets*, ed. D. Burgarella, M. Livio, & C. O'Dea, (Cambridge Univ. Press), 183